Derivation of a scattering model for rarefied gas-solid surface by an unsupervised machine learning approach

NEGF23-434853

DERIVATION OF A SCATTERING MODEL FOR RAREFIED GAS-SOLID SURFACE INTERACTIONS BY AN UNSUPERVISED MACHINE LEARNING APPROACH

S. Mohammad Nejad, S.V. Nedea, and A.J.H. Frijns*
Department of Mechanical Engineering, Eindhoven University of Technology,
PO Box 513, 5600 MB, Eindhoven, The Netherlands

*) corresponding author: a.j.h.frijns@tue.nl

KEYWORDS

Rarefied gas, molecular dynamics (MD) simulation, gas-surface interaction, unsupervised machine learning, Gaussian Mixture model

ABSTRACT

In rarefied gas flows, the non-continuum effects, such as velocity slip and temperature jump commonly appear in the gas layer adjacent to a solid boundary. To simulate the fluid flow in such systems under the moderately rarefied condition, that means a Knudsen number (Kn) less than 0.1, the Navier Stokes (NS) equations may be used but slip boundary conditions should be considered. However, for a higher degree of rarefaction (Kn > 0.1) the NS equations break down and must be substituted by more sophisticated equations such as the Boltzmann equation. Particle-based simulation techniques such as direct simulation Monte Carlo (DSMC) [1], Lattice Boltzmann Method (LBM) [2], and method of moments (MoM) [3] are commonly employed to find approximate solutions to the different forms of the Boltzmann equation. Nevertheless, in all these simulation techniques, rigorous prescription of boundary conditions at solid surfaces is the crucial parameter to guarantee the reliability of the simulation results.

Due to the physical complexity of the interactions at the gas-solid interface, particularly in the case of systems with local nonequilibrium, scattering models with a limited number of parameters cannot completely capture the reflection of gas molecules at the solid boundary. In this work, the Gaussian Mixture (GM) approach, an unsupervised machine learning technique, is employed to construct a gas-surface scattering model [4-7]. The GM scattering model is a parametric model, but unlike the common parametric models, such as Cercignani-Lampis-Lord (CLL) model [8], its performance does not depend on a finite number of parameters, like accommodation coefficients. On the contrary, it retains the flexibility of a nonparametric model, since the whole collision data obtained from the MD simulation is used to train the GM model and no intermediate calibration based on accommodation coefficients is needed. Therefore, this model can capture all the underlying physical phenomena happening at the gas-surface interface

The main input required to train the GM model is the MD collisional data. In the case of monoatomic gases (in this paper we consider an Ar-Au system), having only the translational degrees of freedom, the collisional data is a 6-dimensional dataset consisting of the impinging and outgoing translational velocities of the center of mass (COM) of Ar atoms [5]. For the diatomic gases (in this paper we consider an H_2-Ni system), we must also account for the rotational degrees of freedom. Therefore, the impinging

and outgoing rotational velocities are added to the training data. Here, the final training dataset is a 10-dimensional matrix: the three velocity components and the two rotational speeds for ingoing and outgoing molecules [7]. Benchmarked by MD results, the performance of the GM-driven scattering model is evaluated and compared with the CLL scattering model in a combined Fourier-Couette flow problem in which the cold bottom wall is kept at T_b = 300K, while the hot top wall is kept at T_t = 500K.

The MD simulation setup that is used to generate these data, is schematically shown in Fig.1. It is a two-parallel plate problem. Periodic boundary conditions are applied in x- and z-directions. The distance between the two walls is d =12 nm, for the Ar-Au system, and d = 30 nm for the H_2-Ni system. Each wall is constructed with five layers of FCC planes representing gold and nickel walls for the monatomic and diatomic problems, respectively. The Au wall has a cross-sectional area of 10 nm × 10 nm, while for the Ni wall, the cross-sectional area is 10.8 nm × 10.8 nm. The interactions between the solid Au and Ni atoms located in the walls are models using the corresponding embedded atom model (EAM) potentials developed by Sheng *et al.* [9] and Foiles *et al.* [10], respectively. For the Ar-Au system, the non-bonded gas-gas, and gas-wall interactions are modeled by 12-6 Lennard-Jones potentials ($\varepsilon_{Ar-Ar} = 1.22\ 10^{-2}$ eV; $\sigma_{Ar-Ar} = 3.35$ Å; $\varepsilon_{Ar-Au} = 1.14\ 10^{-2}$ eV; $\sigma_{Ar-Au} = 3.819$ Å) [5]. For the H_2-Ni system, the non-bonded interactions are modeled using COMPASS force field [11], which is a 9-6 Lennard-Jones potential ($\varepsilon_{H-Ni} = 1.19\ 10^{-2}$ eV; $\sigma_{H-Ni} = 2.016$ Å), is applied. For the hydrogen gas-gas interaction the 12-6 Lennard-Jones potential is used ($\varepsilon_{H-H} = 9.29\ 10^{-4}$ eV; $\sigma_{H-H} = 1.421$ Å) [8]. The Knudsen number (Kn) for the Ar-Au system is Kn=0.2 and for the H_2-Ni system is Kn= 0.35. These Knudsen numbers are chosen to be within the transition regime. It was shown for the H_2-Ni system that by increasing the Knudsen number from 0.1 to 0.9 the velocity and energy distributions were not considerably impacted, nor were the corresponding accommodation coefficients (ACs) [12]. Therefore we show here only the results for a single Kn number.

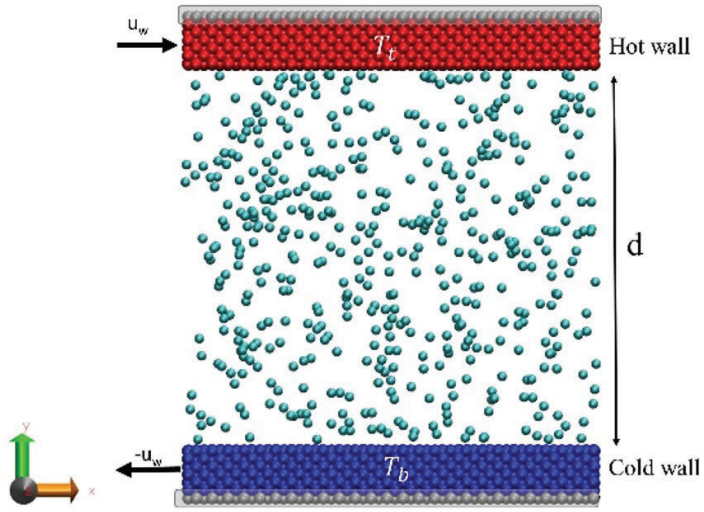

Fig. 1: Schematic representation of the system under consideration for the MD simulations; d: distance between the two walls

As it is depicted in Fig.1, to model the Couette flow condition, walls have been moving with the velocity $u_w = \pm S_w\sqrt{2k_BT_b/m_g}$, where S_w=0.5 and 0.4 for the Ar-Au and H_2-Ni systems, respectively. Various physical and statistical criteria are employed to assess the performance of the applied scattering kernels, including the correlation between the impinging and outgoing velocity components, the probability density function (PDF) of the outgoing velocity components, and the corresponding accommodation coefficients (ACs).

The correlation graphs and PDFs of the translational velocity components for the Ar-Au system at the bottom wall are shown in Fig. 2.

For the CLL scattering kernel, the imposed velocity at the wall is added to all velocity components generated by the CLL kernel in the direction of the wall movement ($V_{x,final} = V_{x,CLL}+u_W$). It is shown that the correlation plots based on both scattering kernels are in good agreement with MD results [5]. However, looking at the predicted PDFs of the outgoing velocity components, mismatches between the CLL and MD results at the peak of the tangential velocity components (V_x,V_z) are observed.

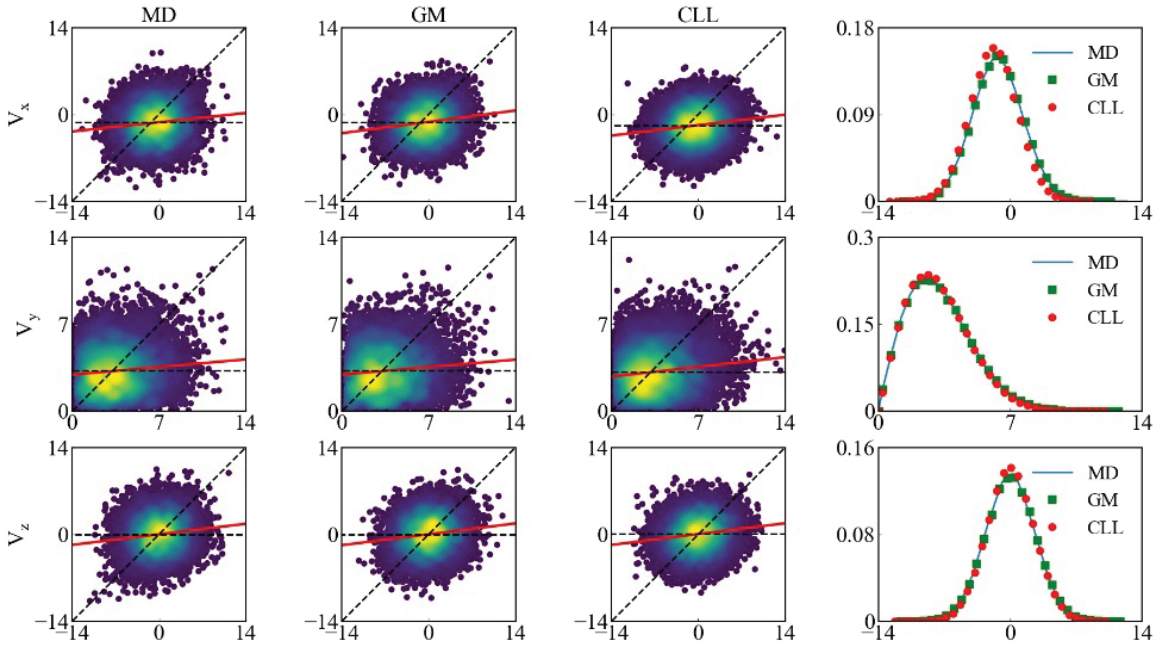

Fig. 2: Velocity correlations of impinging (horizontal-axis) and reflected (vertical-axis) velocity components in Å/ps for the Ar-Au system at the bottom wall [5]. The dashed horizontal and diagonal lines indicate fully diffusive and specular conditions, respectively. Red lines indicate the least-square linear fit of the data. In the last column, the corresponding probability density (PDF) function for the reflecting particles is shown.

The correlation between the impinging and outgoing translational velocity components of the center of mass (V_x;V_y;V_z), different energy modes of the gas molecules (E_{tr};E_{rot} ;E_{tot}), as well as the PDF of the outgoing velocity components or the energy modes for the H_2-Ni system at the bottom wall are presented in Fig.3. It is seen that the results from the GM model are also in good agreement with the MD results. Except for the rotational energy mode, the CLL model does not show a good performance in predicting the other energy modes, nor in predicting the translational velocity components accurately [7].

Using the predicted velocity components by the GM and CLL scattering kernels, the corresponding ACs are computed and compared with the original MD results (see Table.1). For the ACs of different partial velocities ($\alpha_x, \alpha_{y,}\alpha_z$) it is seen that, for the Ar-Au system, the results obtained by both scattering kernels are in good agreement with the MD simulation results [7]. However, it is found that α_{tr} obtained by the CLL model is slightly higher than the MD results, whereas the results obtained by the GM model are always in perfect agreement with the MD ones. For the H_2-Ni system, it is shown that both scattering kernels have an acceptable accuracy in predicting $\alpha_x, \alpha_{y,}\alpha_z$, as well as α_{rot}. However, while the GM model results for α_{tr} and α_{tot} are just slightly higher than the MD results, there is a significant discrepancy between the results obtained from the CLL model and MD simulations.

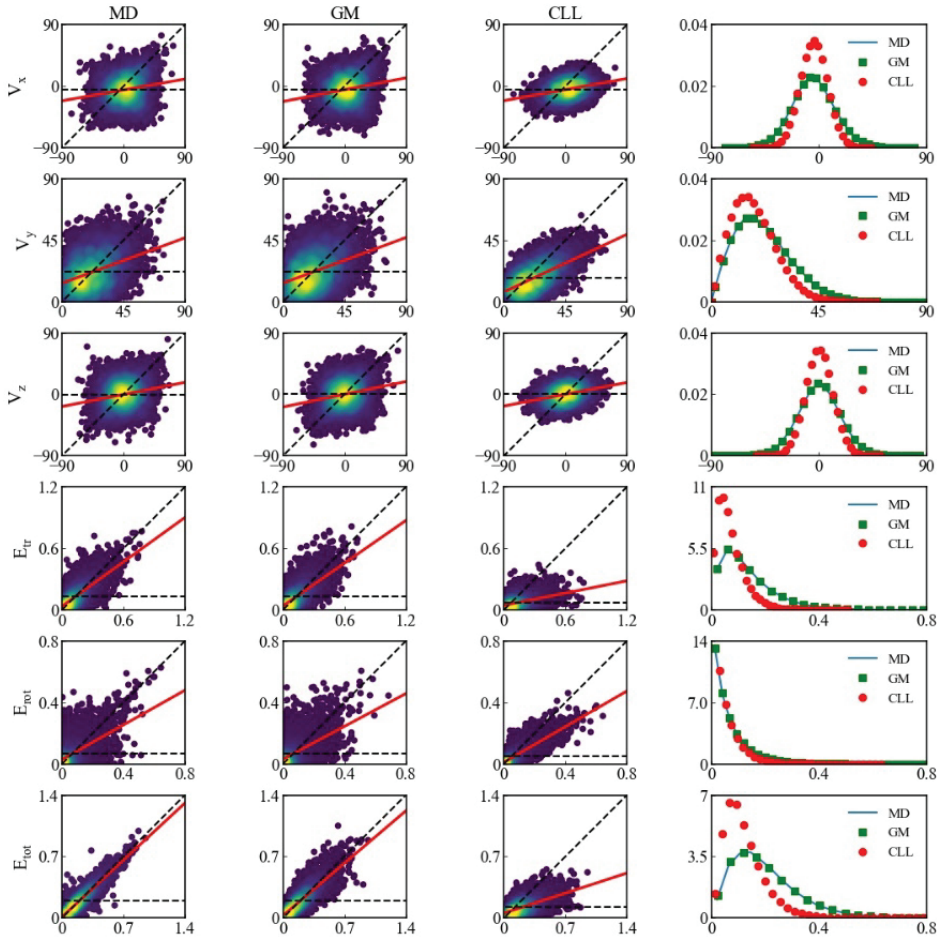

Fig. 3: Correlations between incoming (horizontal-axis) and outgoing (vertical-axis) translational velocity components in [Å/ps] and energy modes in [eV] of combined Fourier-Couette flow problem for the H_2-Ni system at the bottom wall [7]. The dashed horizontal and diagonal lines demonstrate fully diffusive and specular reflection, respectively. Solid red lines demonstrate the least-square linear fit of the kinetic data. In the last column, the corresponding probability density functions of the translational velocity components and energy modes for the reflecting particles are presented

Table 1: Tangential momentum (α_x,α_z), normal momentum (α_y), translational (α_{tr}), rotational (α_{rot}), and total (α_{tot}) energy accommodation coefficients of the combined Fourier-Couette flow problem for the Ar-Au [5] and the H_2-Ni system [7], computed using different scattering kernels: GM and CLL models, and MD simulations.

System	Model	Wall	α_x	α_y	α_z	α_{tr}	α_{rot}	α_{tot}
Ar-Au	MD	bottom	0.876	0.899	0.875	0.869	-	-
		top	0.76	0.78	0.761	0.773	-	-
	GM	bottom	0.877	0.86	0.873	0.877	-	-
		top	0.76	0.79	0.767	0.789	-	-
	CLL	bottom	0.875	0.88	0.873	0.94	-	-
		top	0.76	0.78	0.767	0.897	-	-
H_2-Ni	MD	bottom	0.812	0.633	0.801	0.274	0.418	0.075
		top	0.808	0.646	0.805	0.286	0.420	0.092
	GM	bottom	0.807	0.633	0.802	0.314	0.479	0.155
		top	0.813	0.649	0.807	0.328	0.48	0.167
	CLL	bottom	0.812	0.527	0.80	0.791	0.419	0.667
		top	0.808	0.591	0.804	0.796	0.420	0.670

The observed high precision of the GM predictions indicates that it can be considered a promising candidate to compute important discontinuity phenomena such as temperature jumps and velocity slips in rarefied gas flow systems. In addition, the accuracy of the GM model results indicates the high potential of this approach to construct a generalized scattering kernel for rarefied gas-solid surface interactions. The derived scattering kernels can be directly implemented as boundary conditions to DSMC [13] and the Method of Moments solvers or as slip velocity and temperature jump boundary condition to Navier-Stokes-Fourier solvers.

ACKNOWLEDGEMENTS

This work is funded by the research program RareTrans (NWO-Project No. HTSM-15376).

REFERENCES

[1] G.A. Bird and J.M. Brady (1994) Molecular gas dynamics and the direct simulation of gas flows, volume 5. Clarendon Press Oxford.
[2] J. Zhang (2011) Lattice Boltzmann method for microfluidics: models and applications. *Microfluidics and Nanofluidics*, 10(1):1–28.
[3] C David Levermore (1996) Moment closure hierarchies for kinetic theories. Journal of statistical Physics, 83(5):1021–1065.
[4] M. Liao, Q-D. To, C. Léonard, and W. Yang (2018) Prediction of thermal conductance and friction coefficients at a solid-gas interface from statistical learning of collisions. *Physical Review E*, 98(4):042104.
[5] S. Mohammad Nejad, E. Iype, S. Nedea, A. Frijns, and D. Smeulders (2021) Modeling rarefied gas-solid surface interactions for Couette flow with different wall temperatures using an unsupervised machine learning technique. *Physical Review E*, *104*(1), 015309, https://doi.org/10.1103/PhysRevE.104.015309
[6] H. Wu, W. Chen and Z. Jiang (2022) Gaussian mixture models for diatomic gas-surface interactions under thermal non-equilibrium conditions, *Physics of Fluids* 34, https://doi.org/10.1063/5.0099863
[7] S. Mohammad Nejad, S. Nedea, A. Frijns, and D. Smeulders (2022) Development of a scattering model for diatomic gas-solid surface interactions by an unsupervised machine learning approach. *Physics of Fluids, 34, 117122;* https://doi.org/10.1063/5.0110117
[8] R. Lord (1991) Some extensions to the Cercignani–Lampis gas–surface scattering kernel, *Phys. Fluids A* 3, 706–710.
[9] H. Sheng, H. Kramer, A. Cadien, T. Fujita, and M. Chen (2011) Highly optimized embedded-atom method potentials for fourteen fcc metals, *Physical Review B,* 83, 134118.
[10] S. Foiles, M. Baskes, and M.S. Daw (1986) Embedded-atom-method functions for the fcc metals Cu, Ag, Au, Ni, Pd, Pt, and their alloys, *Physical Review B*, 33, 7983.
[11] H. Sun (1998) Compass: an ab initio force-field optimized for condensed-phase applications overview with details on alkane and benzene compounds, *The Journal of Physical Chemistry B*, 102, 7338–7364.
[12] S. Mohammad Nejad (2023) Scattering dynamics of rarefied gases: a hybrid atomistic/machine learning approach, PhD thesis, Eindhoven University of Technology.
[13] S. Mohammad Nejad, F. Peters, S. Nedea, A. Frijns (2023), A hybrid Gaussian Mixture-DSMC approach applied to the Fourier thermal problem, in: *NEGF23 Proceedings*, paper 434857